Article

A Classical Molecular Dynamics Study of the Effect of the Atomic Force Microscope Tip Shape, Size and Deformation on the Tribological Properties of the Graphene/Au(111) Interface

Cem Maden [1], Hande Ustunel [2,*] and Daniele Toffoli [3,4,*]

[1] Micro and Nanotechnology Programme, Middle East Technical University, 06800 Ankara, Turkey; maden.cem@metu.edu.tr

[2] Department of Physics, Middle East Technical University, 06800 Ankara, Turkey

[3] Dipartimento di Scienze Chimiche e Farmaceutiche, Università degli Studi di Trieste, Via L. Giorgieri 1, 34127 Trieste, Italy

[4] Istituto Officina dei Materiali (IOM)-CNR, S.S.14, km 163.5, 34149 Trieste, Italy

[*] Correspondence: ustunel@metu.edu.tr (H.U.); toffoli@units.it (D.T.)

Abstract: Atomic force microscopes are used, besides their principal function as surface imaging tools, in the surface manipulation and measurement of interfacial properties. In particular, they can be modified to measure lateral friction forces that occur during the sliding of the tip against the underlying substrate. However, the shape, size, and deformation of the tips profoundly affect the measurements in a manner that is difficult to predict. In this work, we investigate the contribution of these effect to the magnitude of the lateral forces during sliding. The surface substrate is chosen to be a few-layer AB-stacked graphene surface, whereas the tip is initially constructed from face-centered cubic gold. In order to separate the effect of deformation from the shape, the rigid tips of three different shapes were considered first, namely, a cone, a pyramid and a hemisphere. The shape was seen to dictate all aspects of the interface during sliding, from temperature dependence to stick–slip behavior. Deformation was investigated next by comparing a rigid hemispherical tip to one of an identical shape and size but with all but the top three layers of atoms being free to move. The deformation, as also verified by an indentation analysis, occurs by means of the lower layers collapsing on the upper ones, thereby increasing the contact area. This collapse mitigates the friction force and decreases it with respect to the rigid tip for the same vertical distance. Finally, the size effect is studied by means of calculating the friction forces for a much larger hemispherical tip whose atoms are free to move. In this case, the deformation is found to be much smaller, but the stick–slip behavior is much more clearly seen.

Keywords: atomic force microscope; friction force microscope; classical molecular dynamics; friction; stick–slip motion

1. Introduction

Beyond its use as an imaging tool, the atomic force microscope (AFM) is also often utilized in the characterization and manipulation of surfaces and surface adsorbates. The use of an AFM tip for surface indentation [1], surface scratching [2] and the displacement of nanoclusters on a surface [3] has now become routine. Additionally, interfacial properties such as the energy of adhesion can also be determined via the pull-off force experienced by the tip as it is being moved away from a surface [4]. Among the various such uses of an AFM tip, a prominent one is the friction force microscopy (FFM) [5], where the tip is modified to measure lateral forces at an interface of two materials in relative motion. This function enables the understanding and identification of low-friction interfaces and lubricants. For instance, in recent years, two-dimensional materials have emerged as excellent lubricants with very low friction [6–9].

The foundations of the atomic scale description of sliding friction date back to the late 1920s. The earliest model developed simultaneously by Prandtl [10] and Tomlinson [11] is a simplified representation of an AFM tip sliding on a surface, where the cantilever and the tip have been replaced by two point masses connected by a spring. The substrate over which the tip slides, on the other hand, is described by a sinusoidal potential energy surface (PES). This simple model reveals the characteristic stick–slip motion, where the tip is periodically trapped in the pits of the PES and is released when the elastic energy build-up in the spring is large enough to overcome the barrier. Since the Prandtl–Tomlinson model was proposed, there have been more sophisticated models developed over the years, most notably by Frenkel, Tomlinson, and Kontorova [12], Sokoloff [13,14], and Zhong and Tomanek [15]. However, the stick–slip behavior has always been a common theme in all models proposed. The chemical composition and the physical morphology of the tip, which is largely ignored in these simple models, has proven to be a crucial element for understanding and controlling interfacial phenomena via an AFM [16]. Friction investigations often include a mapping of the interfacial PES; however, the morphology of the PES depends on the properties of both the components making up the interface. For instance, the stick–slip motion depends on both the material that the AFM tip is made of and the surface [17]. Ko et al. [18] showed that tips made out of metal alloys show different shear and adhesion behavior during sliding depending on whether the alloy is miscible or immiscible. Dong et al. [19] observed, through AFM measurements and MD simulations, that the size and the shape of the tip affect the lateral forces when moving up and down surface steps of graphite. Furthermore, the size and the shape of the actual contact area also depends upon the vertical load applied to the AFM tip, which in turn affects the PES [20]. Further complications may occur due to the presence of an interfacial fluid, such as water or a lubricant [21] as well as wear and material consumption due to friction [22].

Due to the aforementioned sensitive dependence on the experimental parameters of the measurements, computational tools such as density functional theory and molecular dynamics (MD) have become indispensable in understanding the atomistic picture underneath the operation of the AFM tip [1,16]. Among such studies, some notable examples are as follows. In the MD simulation by Korayem et al. [23], the manipulation of a Au nanoparticle by a Ag tip on a Ag substrate in the absence and presence of a water meniscus was studied. Jacobs et al. [4] used a continuum model along with MD simulations and experimental TEM data to understand the effect of surface roughness on the pull-off force of H-saturated diamond tips. Hu et al. [24] studied, via MD simulations, the nanoscale wear of a silicon dioxide tip sliding on a copper substrate. Reischl et al. [25] used simulated AFM images generated by the postprocessing of MD data to understand whether a carbon nanotube tip can resolve individual point defects on a surface covered with explicit water. Kopycinska-Müller et al. [26] demonstrated that a Si tip will undergo a phase change under load. Xu et al. [16] conducted MD simulations of a 10 nm-radius melt-quenched Pt tip sliding on a Au(111) surface. They noted that in the presence of neighboring grains, irregular stick–slip occurs, whereas if the tip is a grain-free single crystal, the stick–slip is much more regular. Xu et al. [27] studied, using MD, the stick–slip signature of the amorphous silica tip on the Au(111) surface. A small and a large tip were prepared and used for recording lateral forces. For the small tip, a high-friction regime appears for loads larger than a threshold value, which is attributed to surface defects.

Several aspects of the sliding of AFM tips on graphene substrates have been studied in the literature. Our work aims to address two issues that have been the subject of relatively fewer studies: the effect of the shape and size of the AFM tip and the use of a metal as an AFM tip. In most studies, hemispherical semiconductor tips are modeled. In our paper, molecular dynamics simulations were used to explore the effect of the size, shape and deformation of AFM tips in the determination of the sliding friction force. To study the effect of shape, Au tips of three different geometries, namely, a cone, a hemisphere and a pyramid, were chosen, and the friction forces while sliding on the same few-layer graphene substrate were compared. The choice of Au as the tip material is motivated by the fact

that although conducting tips are important for such applications as sensing [28], very few studies are devoted to metal tips. For the dependence on load, three different heights were chosen, and average friction forces were calculated. Rigid and plastically deformable hemispherical tips were then compared to understand the effect of deformation. In addition to friction force calculations, indentation analyses were conducted as well. Two different sizes were studied for the hemispherical tip in order to understand size dependence.

2. Materials and Methods

The MD simulations presented in this paper were performed using the open-source software suite Large-Scale Atomic/Molecular Massively Parallel Simulator (LAMMPS) [29]. Bonded and non-bonded Au-Au and C-C were modeled using the Embedded Atom Model (EAM) [30], and Adaptive Intermolecular Reactive Empirical Bond Order (AIREBO) [31] force fields, respectively. The non-bonded interaction between Au and C is described using the Lennard-Jones 12-6 potential [32], where the interaction potential energy between atoms i and j is described by

$$E(r_{ij}) = 4\varepsilon \left[\frac{\sigma^6}{r_{ij}^6} - \frac{\sigma^{12}}{r_{ij}^{12}} \right] \tag{1}$$

where r_{ij} is the interatomic distance, while ε and σ are the model parameters that are related to the bond energy and bond length, respectively. For this work, σ and ϵ were taken from previous work [33] to be 3.003 Å and 0.0341 eV, respectively. Atoms that are further apart from one another than 15 Å were excluded from the calculation and considered noninteracting.

In our MD simulations, the equations of motion were integrated using the velocity Verlet algorithm [34] with a time step of 1 fs. Temperature control was achieved via the Berendsen thermostat [35]. The surface was modeled by a slab of four ABAB-stacked graphene layers where periodic boundary conditions were imposed on the plane of the surface. Throughout the simulations, the bottom two layers were fixed, while the top two layers were allowed to move according to the equations of motion. The indentation study, however, was conducted on a six-layer graphene substrate with two of the bottommost layers fixed.

The shape effect study was conducted by employing tips of three geometric shapes, namely, a cone, a pyramid and a hemisphere, as represented by the first three models in Figure 1a. During the sliding simulations, the Au atoms in all three tips were kept at rigid positions with respect to one another to exclude deformation effects. The instantaneous lateral force profiles and average forces were compared for three different tip heights (roughly corresponding to three loads) and three different temperatures (T = 1 K, 100 K, and 300 K). Next, deformation was included by relaxing the constraints to all but the top three layers of the hemispherical tip (leftmost tip in Figure 1a) and allowing the lower atoms to move during the simulations. The numbers of Au atoms in the conical, pyramidal, and hemispherical tips are 71, 285, and 372, respectively. With a 13 Å radius, the nonrigid tip contains 198 mobile Au atoms. To further elucidate the deformation, an indentation simulation, where the nonrigid hemispherical tip was steadily lowered onto the surface by about 3.5 Å without sliding, was conducted. Finally, to explore the size effect, a larger hemisphere with a radius of 30 Å was also built, where only the top three layers were taken to be fixed. This tip includes 2966 Au atoms, of which 1816 are mobile (Figure 1b). All tips were created from the face-centered cubic phase of Au. For the smaller tips, a 120 Å × 123 Å underlying graphene substrate with 22,736 C atoms was used (Figure 1c). For the largest tip, the substrate surface area was extended to approximately 221 Å × 221 Å with 74,880 C atoms.

During the sliding simulations, lateral friction forces were calculated by means of pulling the tips along the surface at a predetermined height with a constant velocity and recording the component of the forces in the opposite direction to the motion. The average of the magnitude of the lateral forces was then calculated and reported for comparison.

To understand the effect of increasing load, sliding simulations were conducted at different heights. In this context, the height h is defined to be the distance between the topmost fixed layer of the tip and the bottommost fixed layer of the surface. For the fixed tips, three heights h_1, h_2, and h_3 Å were considered, which correspond to distances of 2.0 Å, 2.5 Å and 3.0 Å from the lowest point of the tip to the top of the unperturbed surface, respectively. Since each rigid tip consists of a different number of layers, h_1, h_2, and h_3 are all different for the three tips, which are listed in Table 1. For the nonrigid hemispherical tip, we consider three different distances of $h_4 = 24.27$ Å, $h_5 = 24.77$ Å, and $h_6 = 25.27$ Å; however, the translation of these distances to the bottom of the tip-to-surface distance is ambiguous due to deformations. In order to compare sliding along different directions, all tips except for the large hemisphere tips were dragged along the x axis (moving parallel to the C-C bonds) and the y axis (moving perpendicular to the C-C bonds) for each load and temperature.
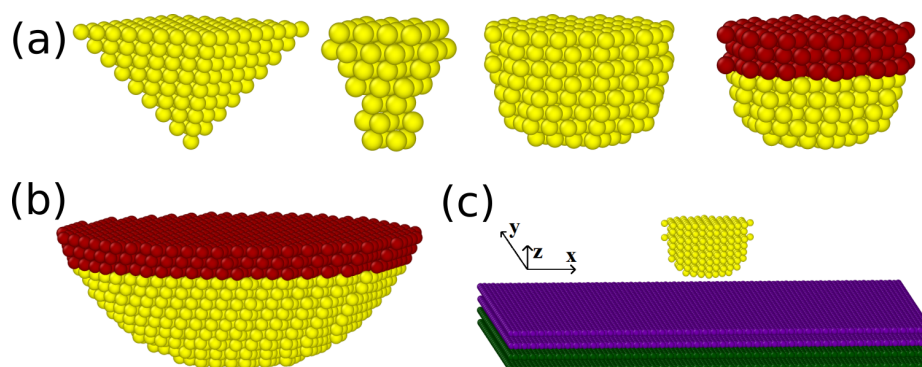

Figure 1. Smaller (**a**), and larger (**b**) models for the AFM tip. Of the smaller tips, the ones that are represented only with yellow spheres are completely fixed during the simulations. The shapes of the smaller tips are pyramidal, conical, and hemispherical from left to right. The larger spherical tip is shown in (**b**). The smaller rigid hemispherical tip together with the graphene substrate is shown in (**c**). Yellow and red spheres represent Au atoms. Red spheres, in particular, correspond to atoms that are fixed in two hemispherical tips. Magenta and green spheres represent free and fixed carbon atoms in the substrate.

Table 1. Tip heights h_1, h_2 and h_3 (in Å) for the three rigid tips. The definitions of these heights are given in the text.

Heights	Pyramidal	Conical	Hemispherical
h_1	28.36	24.27	26.35
h_2	28.86	24.77	26.85
h_3	29.36	25.27	27.35

The MD protocol followed in the preparation and production stages of our calculations can be summarized as follows: Before any sliding or indentation simulations were initiated, the mobile atoms of the substrate were gradually heated from 1 K to the target temperature in an NVT ensemble. The system was then kept at an NVT ensemble at the target temperature for 1 ns. After this thermalization stage was complete, the tip was brought closer to the substrate slowly. A further thermalization step was conducted before the sliding or indentation process at the target temperature. Afterwards, sliding/indentation was initiated at the prescribed speeds while continuing to control the temperature within an NVT ensemble. As a test, in one of the sliding simulations, the thermostat was turned off, and the system was allowed to evolve in an NVE ensemble. The results were seen to be unaffected, and therefore the NVT ensemble was employed in all simulations.

During sliding, all tips were along on the substrate for 10 Å with a velocity of 10 cm/s except for the large hemispherical tip, which moved at a speed of 1 m/s. All sliding simulations were carried on for a total of 10 ns. In the indentation simulation, the tip was displaced down the z axis (normal to the surface).

3. Results

Rigid AFM tips in the shape of a pyramid, a cone, and a hemisphere were pulled along the x and y directions as defined in Figure 1c at three different heights of h_1, h_2, and h_3 with a speed of 10 cm/s at temperatures of 1 K, 100 K, and 300 K. The average vertical loads (F_N) corresponding to these three heights and for all temperatures for all rigid tips are listed in Table 2 in nN. The largest distance (h_3) results in negative loads, which correspond to the case of the surface lifting upwards towards the tip due to van der Waals forces. The magnitude of the vertical load is seen to increase with temperature for all shapes and heights but for a few exceptions. There is no perceptible dependence on the sliding direction.

Table 2. Average vertical load, F_N, in nN for the three rigid tips at T = 1 K, 100 K, 300 K for three heights and two sliding directions. h_1, h_2 and h_3 are defined in Table 1. The sliding speed is 10 cm/s.

	Along x			Along y		
Pyramid	1 K	100 K	300 K	1 K	100 K	300 K
h_1	2.521	2.636	2.829	2.525	2.643	2.833
h_2	0.264	0.348	0.510	0.282	0.362	0.515
h_3	−0.904	−0.856	−0.756	−0.878	−0.830	−0.723
Cone	1 K	100 K	300 K	1 K	100 K	300 K
h_1	8.072	8.300	8.727	8.034	8.281	8.714
h_2	2.90	2.466	2.799	2.252	2.420	2.738
h_3	−0.782	−0.664	−0.401	−0.815	−0.688	−0.427
Hemisphere	1 K	100 K	300 K	1 K	100 K	300 K
h_1	16.697	17.253	18.270	16.567	17.111	18.131
h_2	2.116	2.526	3.27	2.210	2.619	3.379
h_3	−4.010	−4.590	−4.886	−3.908	−4.496	−4.792

The horizontal friction forces measured during sliding as a function of distance are shown for the rigid AFM tips with three different shapes along the x and y directions, and those for the three temperatures involved (T = 1 K, 100 K, 300 K) are shown in Figures S1–S3 of the Supplementary Material (SM). From these results, it is immediately obvious that the shape of the tip makes a very significant difference in the friction measurements. Starting first with the common features in the T = 1 K results in Figure S1, the energy barriers for the tip to overcome that occur along the y direction (i.e., against C-C bonds) are much larger than those along the x direction for all tip shapes but the pyramid. This difference is particularly pronounced for the conical tip. The maximum force encountered while sliding along the y direction is approximately ten times the force along the x axis. For the pyramid, the vertical force displays a double-peak character along the y axis, which is not seen in any of the other tips studied here. For this tip, only a single atom at the edge of the tip is in direct contact with the surface. As a result, the lateral friction force profile is a good representation of the actual potential energy surface along the x and y directions of the underlying substrate. The single atom at the end of the tip is positioned such that it actually passes over atoms in a maximum-overlap configuration, and sliding starts at a hexagonal hollow site of the surface. This means that the double peak feature corresponds

to the single tip sliding over one atom and then the next at either end of a C-C bond. Finally, the hemisphere displays the well-known stick–slip pattern for the two smallest vertical distances while sliding along the y-axis. This is also seen to a certain extent for the cone but is much more pronounced for the hemisphere. In an actual sliding experiment, the stick–slip occurs due to both the elastic properties of the tip and the substrate [7], whereas in the present case of rigid tips, we only observe the effect of the substrates. At T = 100 K, the periodic structure of the lateral force with well-defined peaks is mostly lost for the cone and the hemisphere for sliding along the x direction due to increased thermal motion of the atoms. In all other cases, the sinusoidal pattern is maintained with some noise. At T = 300 K, the noise increases, but the pattern from T = 100 K is maintained for all tips in both directions. For instance, for the hemisphere, the stick–slip pattern is persistent at all temperatures along the y direction. The increase in the friction with increasing temperature is partially attributed to the increasing load for a given height as shown in Table 2. In addition, the potential energy surface wells appear to deepen with increasing temperature due to the added mobility of the graphene atoms, which allow the rigid tips to go further into the underlying substrate.

Next, we present and compare our results for average total lateral forces for all tips and temperatures with the goal of understanding whether the differences seen in the sliding characteristics for the different tips are still present when averaged over the total sliding distance. The average friction force for all heights, temperatures and shapes is given in Table 3, and trends are shown as plots in Figure 2.

Table 3. Average lateral friction force F_f in nN for the three rigid tips at T = 1 K, 100 K, 300 K for three heights and two sliding directions. h_1, h_2 and h_3 are defined in the text. The sliding speed is 10 cm/s.

|	**Along x**			**Along y**		
Pyramid	1 K	100 K	300 K	1 K	100 K	300 K
h_1	0.0960	0.1312	0.1883	0.0811	0.1276	0.1953
h_2	0.0824	0.0933	0.1165	0.0646	0.0822	0.1103
h_3	0.0384	0.0427	0.0519	0.0303	0.0359	0.0464
Cone	1K	100 K	300 K	1 K	100 K	300 K
h_1	0.0164	0.1240	0.2246	0.2815	0.3031	0.3537
h_2	0.0121	0.0641	0.1175	0.1744	0.1831	0.2085
h_3	0.0160	0.0286	0.0509	0.0896	0.0951	0.1079
Hemisphere	1 K	100 K	300 K	1 K	100 K	300 K
h_1	0.0638	0.1979	0.3481	1.1776	1.0498	1.1520
h_2	0.0573	0.1179	0.2042	0.6938	0.7159	0.7563
h_3	0.0242	0.0597	0.1095	0.4146	0.4277	0.4564
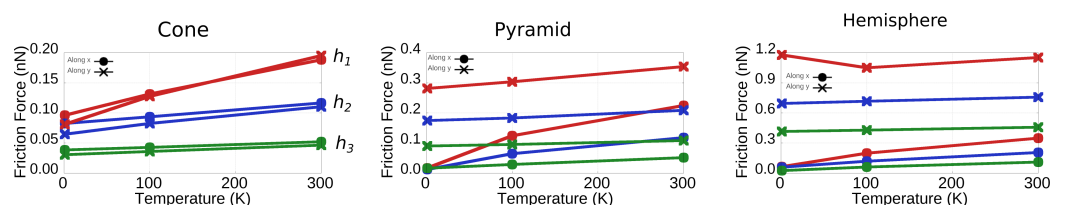
Figure 2. Trends in average friction force as a function of temperature for three different rigid tips (top to bottom: cone, pyramid, and hemisphere) for three different heights (h_1 red lines, h_2 blue lines, and h_3 green) and for sliding in two different directions (solid circles for x and crosses for y). The speed of sliding is 10 cm/s.

Unlike the average vertical load, the friction behavior shows significant variation across the parameter space. A common observed trend is the increase in friction with increasing temperature. For the cone, the average lateral force along the x and y directions is nearly identical at all heights and all temperatures. For the pyramid and the hemisphere, however, the y direction yields lower lateral forces.

Next, we consider the effect of deformation. For this part of our investigation, we consider a hemispherical tip with only the top three layers fixed, while all the atoms in the remaining layers are free to move. Figure 3 shows the completely rigid hemispherical tip described above along with a tip with only the top three layers fixed. The height of the tips in this figure correspond to h_5 as defined in the Methods section. The sizable deformation of the nonrigid tip is already seen clearly for this size. The initial five layers that taper off down the tip are now merged into four evenly sized layers, increasing the contact area between the tip and the surface. As a result, the inward depression of the top surface layers visible for the rigid tip disappears for the nonrigid tip.
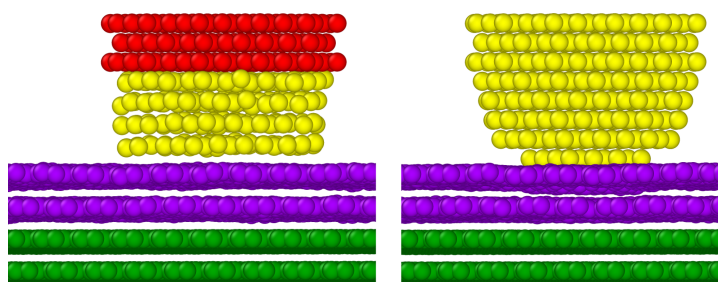

Figure 3. (**Left panel**): Hemispherical tip with three top layers fixed, with the rest of the atoms free to move. (**Right panel**): Completely rigid hemispherical tip. Red and yellow spheres represent the fixed and free Au atoms. Green and magenta spheres represent fixed and free carbon atom layers.

The lateral forces measured as a function of sliding distance along x and y at T = 300 K and three heights h_4, h_5, and h_6 are shown in Figure 4. Interestingly, the behavior of the rigid and nonrigid tips are very similar as far as the lateral forces are concerned (compare Figure 4 with Figure S3 of the Supplementary Materials). The stick–slip pattern is more pronounced for the nonrigid tip in comparison to the rigid one. Evidently, the added elasticity of the tip will contribute to the build up of the forces in the stick phase, increasing the abruptness of the slip.
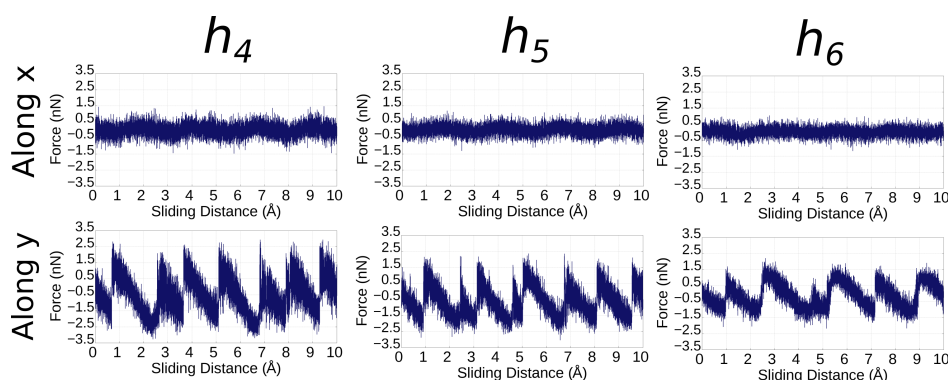

Figure 4. The lateral friction force along the x direction (**top panels**) and the y direction (**bottom panels**) for a flexible (nonrigid) tip sliding with a speed of 10 cm/s at T = 300 K.

The average vertical loads (F_N) and average lateral friction forces (F_f) at heights h_4, h_5, and h_6 are shown in Table 4 for a temperature of T = 300 K. Although the heights are not the same for the rigid and the nonrigid tips, the overall magnitudes of the lateral friction forces are similar. For a hemispherical tip of this size then, the effect of the deformation is moderate.

Table 4. Average load F_N and lateral friction F_f forces in nN for the nonrigid hemisphere shape at three distances and at a temperature of T = 300 K.

Height [Å]	Along x		Along y	
	F_N	F_f	F_N	F_f
h_4	5.780	0.305	6.843	1.175
h_5	1.669	0.254	1.731	1.086
h_6	−2.299	−0.221	3.012	0.689

In order to further understand the deformation of a tip under heavier loads, we conduct an MD simulation at 300 K in which the hemispherical tip approaches a six-layer graphene surface from the top. We then monitor the deformation via the mean square displacement of the graphene layers. An animation of this motion is provided as a part of the Supplementary Materials. Different stages of the tip during its descent onto the surface are reported in Figure 5. During the approach, atoms on the outer layer of the tip are seen to climb up the tip along the sides. The upward displacement of the Au atoms in groups occurs suddenly as seen by jumps in the means square displacement of the graphene layers seen in Figure 5. In this figure, the mean square displacement from equilibrium for the top four mobile layers of graphene is shown. As the tip presses onto the surface, all layers first are compressed downward slightly and continuously. At around 3.1 Å of tip displacement, the top layer experiences a sudden displacement of more than 1 Å, which corresponds to the displacement of the bottom layer of the tip in the upward direction. The second and third layers from the top also experience a displacement at this point but by a much smaller amount. Just before the tip reaches a displacement of 3.5 Å, the top layer experiences another sudden displacement by a small amount; by this time, the large displacement is also seen in the second and third layers as well. Throughout this motion, the fourth layer remains mostly unperturbed.
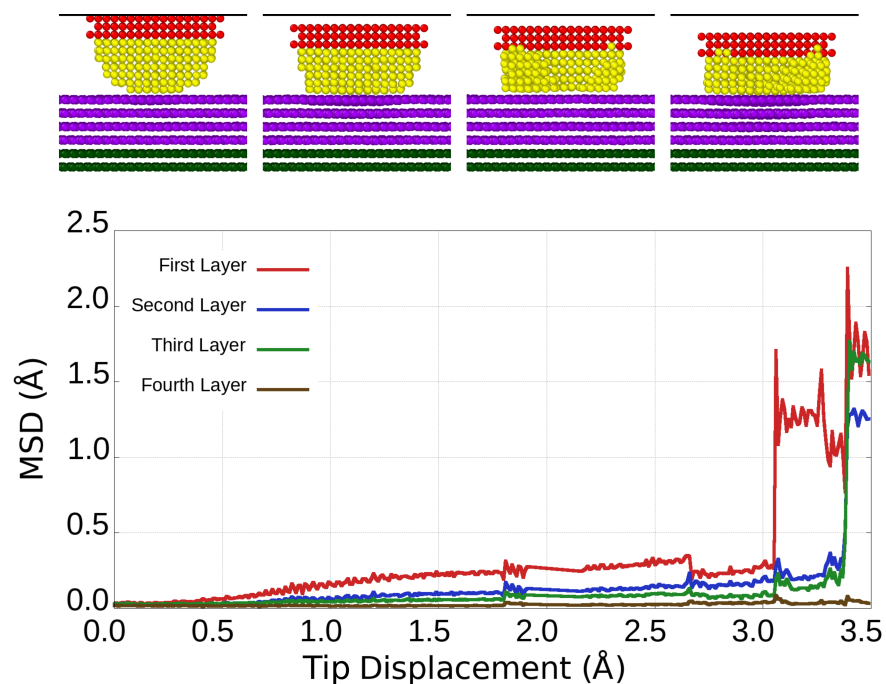
Figure 5. (**Top panels**): Hemispherical tip in an indentation sequence descending onto a 6-layer graphene surface. (**Bottom panel**): Mean square displacement of atoms on each of the top four graphene layers. Red and yellow spheres represent the fixed and free Au atoms. Green and magenta spheres represent fixed and free carbon atoms.

Finally, in Figure 6a, the largest tip with the three top layers fixed is shown during sliding at a distance of approximately 1 Å between the bottom of the tip and the top graphene layer. At this distance, the vertical load as a function of sliding distance along the y direction is shown in Figure 6b with an average value of 4.92 nN. The lateral friction force as a function of sliding distance, on the other hand, is shown in Figure 6c with an average of 2.2 nN.
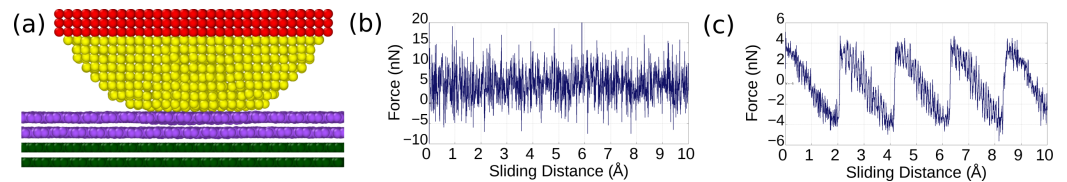

Figure 6. (**a**) Large hemispherical tip sliding at speed 1 m/s and at a temperature of 300 K with the closest distance between the tip and the surface being approximately 1 Å. (**b**) Average vertical load as a function of the sliding distance. (**c**) Average friction force as a function of the sliding distance. Red and yellow spheres represent the fixed and free Au atoms. Green and magenta spheres represent fixed and free carbon atoms.

At this distance, the deformation in the tip is much smaller than the smaller tip. The upward motion of the atoms is much smaller and, most importantly, the stick–slip motion is much more visible. At this scale, our results can be compared to the experimental measurements. For instance, in the AFM-assisted sliding friction measurements by Ptak et al. [36], a Si tip with a radius of 10 nm was used to measure the sliding friction of HOPG graphene. This size is comparable to our largest tip, and the amplitude and the period of the stick pattern in our work agrees very well with the measurements in this work.

4. Discussion and Conclusions

In this work, we have explored, through finite temperature classical molecular dynamics, the effect of the shape, size, and deformation of the tip on the AFM reading during the sliding of the tip on a surface. Due to the desirable properties of layered materials as lubricants, we used a few-layer graphene substrate as the surface and Au tips of various shapes and sizes.

In order to separate the effect of the shape from that of tip deformation, we first considered three completely rigid tips of different shapes, namely, a cone, a pyramid, and a hemisphere. The vertical load, sliding direction, and surface temperature were also included as parameters of the problem. The shape is seen to affect all aspects of the AFM readings. Some notable observations can be summarized as follows: The conical tip, terminating in a single atom, shows identical behavior along the x and y directions. The rigid hemisphere, on the other hand, shows three to four times more resistance to sliding along the y-axis than the x-axis. For the pyramidal tip, directional divergence of the friction force behavior is moderate. The signature stick–slip behavior of atomic-scale friction is more or less prominent depending on the shape of the tip as detailed in the Results section.

The effect of deformation was explored using two hemispherical tips, one with only three layers fixed from the top and one completely rigid. The two tips start out identical but during sliding at different distances, the nonrigid tip experiences significant deformation. The mode of the deformation is the upwards motion of the lower layers of the tip and a flattening of the curved surface, thereby increasing the contact area. A comparison between the behavior of the rigid and nonrigid tip reveals a smaller average load and smaller average friction force for similar distances between the top layer of the tip and the top surface layer. This is, of course, due to the freedom of the lower layers that are free to move upwards and mitigate the vertical load.

The details of the deformation were further analyzed by means of an indentation experiment. The same nonrigid hemispherical tip was monitored as it approached a slightly thicker few-layer graphene surface. The mean square displacement of the graphene layers, which was monitored throughout the experiment, reveals that deformation occurs through the sudden combined jumps of several atoms that relieves the underlying graphene, causing an upward jump. While the topmost layer of the graphene layer is affected the most, as the distance between the tip and the graphene surface decreases, the second and third layers are equally affected.

Finally, the size of the tip was also explored. During sliding, the larger hemisphere exhibits a much smaller degree of deformation. At the same time, the stick–slip pattern is clearer than the smaller hemisphere.

Abbreviations

The following abbreviations are used in this manuscript:

PES	Potential energy surface
LAMMPS	Large-scale Atomic/Molecular Massively Parallel Simulator
EAM	Embedded Atom Model
AIREBO	Adaptive Intermolecular Reactive Empirical Bond Order
MD	Molecular Dynamics

References

1. Uzoma, P.C.; Ding, X.; Wen, X.; Zhang, L.; Penkov, O.V.; Hu, H. A wear-resistant silicon nano-spherical AFM probe for robust nanotribological studies. *Phys. Chem. Chem. Phys.* **2022**, *24*, 23849–23857. [CrossRef]
2. Hu, J.; He, Y.; Li, Z.; Zhang, L. On the deformation mechanism of SiC under nano-scratching: An experimental investigation. *Wear* **2023**, *522*, 204871. [CrossRef]
3. Tripathi, M.; Paolicelli, G.; Daddato, S.; Valeri, S. Controlled AFM detachments and movement of nanoparticles: Gold clusters on HOPG at different temperatures. *Nanotechnology* **2012**, *23*, 245706. [CrossRef]
4. Jacobs, T.D.; Ryan, K.E.; Keating, P.L.; Grierson, D.S.; Lefever, J.A.; Turner, K.T.; Harrison, J.A.; Carpick, R.W. The effect of atomic-scale roughness on the adhesion of nanoscale asperities: A combined simulation and experimental investigation. *Tribol. Lett.* **2013**, *50*, 81–93. [CrossRef]
5. Marsden, A.J.; Phillips, M.; Wilson, N.R. Friction force microscopy: A simple technique for identifying graphene on rough substrates and mapping the orientation of graphene grains on copper. *Nanotechnology* **2013**, *24*, 255704. [CrossRef] [PubMed]
6. Baksi, M.; Toffoli, D.; Gulseren, O.; Ustunel, H. Nanotribological Properties of the h-BN/Au(111) Interface: A DFT Study. *J. Phys. Chem. C* **2019**, *123*, 28411–28418. [CrossRef]
7. Ustunel, H.; Toffoli, D. Tribology at the atomic scale with density functional theory. *Electron. Struct.* **2022**, *4*, 023002. [CrossRef]

8. Song, Y.; Meyer, E. Atomic Friction Processes of Two-Dimensional Materials. *Langmuir ACS J. Surfaces Colloids* **2023**, *39*, 15409–15416. [CrossRef] [PubMed]

9. Huang, P.; Deng, W.; Qi, W.; Chen, X.; Tian, J.; Wang, Y.; Li, X.; Xu, J.; Zhang, C.; Luo, J. Superlow friction and wear enabled by nanodiamond and hexagonal boron nitride on a-C:H films surfaces in dry nitrogen. *Mater. Today Nano* **2023**, *24*, 100384. [CrossRef]

10. Prandtl, L. Ein gedankenmodell zur kinetischen theorie der festen körper. *J. Appl. Math. Mech.* **1928**, *8*, 85. [CrossRef]

11. Tomlinson, G. CVI. A molecular theory of friction. *Lond. Edinb. Dublin Philos. Mag. J. Sci.* **1929**, *7*, 905–939. [CrossRef]

12. Frenkel, Y.; Kontorova, T. On the Theory of Plastic Deformation and Twinning. II. *Phys. Z. Sowjetunion* **1938**, *8*, 1340–1348.

13. Sokoloff, J.B. Theory of energy dissipation in sliding crystal surfaces. *Phys. Rev. B* **1990**, *42*, 760–765. [CrossRef]

14. Sokoloff, J.B. Theory of Energy Dissipation in Sliding Crystal Surfaces at Nonzero Temperature. *Phys. Rev. B* **1993**, *47*, 6106–6109. [CrossRef] [PubMed]

15. Tomanek, D.; Zhong, W.; Thomas, H. Calculation of an Atomically Modulated Friction Force in Atomic-Force Microscopy. *Europhys. Lett* **1991**, *15*, 887–892. [CrossRef]

16. Xu, R.G.; Zhang, G.; Xiang, Y.; Garcia, J.; Leng, Y. Will Polycrystalline Platinum Tip Sliding on a Gold(111) Surface Produce Regular Stick-Slip Friction? *Langmuir* **2022**, *38*, 6808–6816. [CrossRef] [PubMed]

17. He, Y.; She, D.; Liu, Z.; Wang, X.; Zhong, L.; Wang, C.; Wang, G.; Mao, S.X. Atomistic observation on diffusion-mediated friction between single-asperity contacts. *Nat. Mater.* **2022**, *21*, 173–180. [CrossRef]

18. Ko, H.E.; Kwan, S.G.; Park, H.W.; Caron, A. Chemical effects on the sliding friction of Ag and Au(111). *Friction* **2018**, *6*, 84–97. [CrossRef]

19. Dong, Y.; Liu, X.Z.; Egberts, P.; Ye, Z.; Carpick, R.W.; Martini, A. Correlation between probe shape and atomic friction peaks at graphite step edges. *Tribol. Lett.* **2013**, *50*, 49–57. [CrossRef]

20. Vishnubhotla, S.B.; Chen, R.; Khanal, S.R.; Martini, A.; Jacobs, T.D. Understanding contact between platinum nanocontacts at low loads: The effect of reversible plasticity. *Nanotechnology* **2019**, *30*, 035704. [CrossRef] [PubMed]

21. Tian, S.; Chen, X.; Yuan, Q. Shape optimization of a meniscus-adherent nanotip. *Nanoscale* **2023**, *15*, 11099–11106. [CrossRef]

22. Gosvami, N.N.; Feldmann, M.; Peguiron, J.; Moseler, M.; Schirmeisen, A.; Bennewitz, R. Ageing of a Microscopic Sliding Gold Contact at Low Temperatures. *Phys. Rev. Lett.* **2011**, *107*, 144303. [CrossRef] [PubMed]

23. Korayem, M.H.; Hefzabad, R.N.; Homayooni, A.; Aslani, H. Molecular dynamics simulation of nanomanipulation based on AFM in liquid ambient. *Appl. Phys. A Mater. Sci. Process.* **2016**, *122*, 977. [CrossRef]

24. Hu, X.; Tourek, C.J.; Ye, Z.; Sundararajan, S.; Martini, A. Structural and chemical evolution of the near-apex region of an atomic force microscope tip subject to sliding. *Tribol. Lett.* **2014**, *53*, 181–187. [CrossRef]

25. Reischl, B.; Raiteri, P.; Gale, J.D.; Rohl, A.L. Can Point Defects in Surfaces in Solution be Atomically Resolved by Atomic Force Microscopy? *Phys. Rev. Lett.* **2016**, *117*, 226101. [CrossRef] [PubMed]

26. Kopycinska-Müller, M.; Barth, M.; Küttner, M.; Köhler, B. Phase transformation in AFM silicon tips. *Nanotechnology* **2017**, *28*, 355701. [CrossRef]

27. Xu, R.G.; Zhang, G.; Xiang, Y.; Leng, Y. On the Friction Behavior of SiO_2 Tip Sliding on the Au(111) Surface: How Does an Amorphous SiO_2 Tip Produce Regular Stick-Slip Friction and Friction Duality? *Langmuir* **2023**, *39*, 6425–6432. [CrossRef]

28. Abbas, Y.; Rezk, A.; Saadat, I.; Nayfeh, A.; Rezeq, M. Photodetection Characteristics of Gold Coated AFM Tips and n-Silicon Substrate nano-Schottky Interfaces. *Sci. Rep.* **2019**, *9*, 13586. [CrossRef]

29. Plimpton, S. Fast Parallel Algorithms for Short-Range Molecular Dynamics. *J. Comput. Phys.* **1995**, *117*, 1–19. [CrossRef]

30. Daw, M.S.; Baskes, M.I. Embedded-atom method: Derivation and application to impurities, surfaces, and other defects in metals. *Phys. Rev. B* **1984**, *29*, 6443–6453. [CrossRef]

31. Stuart, S.J.; Tutein, A.B.; Harrison, J.A. A reactive potential for hydrocarbons with intermolecular interactions. *J. Chem. Phys.* **2000**, *112*, 6472–6486. [CrossRef]

32. Jones, J.E.; Chapman, S. On the determination of molecular fields. II. From the equation of state of a gas. *Proc. R. Soc. Lond. Ser. A Contain. Pap. Math. Phys. Character* **1924**, *106*, 463–477.

33. Neek-Amal, M.; Asgari, R.; Tabar, M.R.R. The formation of atomic nanoclusters on graphene sheets. *Nanotechnology* **2009**, *20*, 135602. [CrossRef] [PubMed]

34. Verlet, L. Computer "Experiments" on Classical Fluids. I. Thermodynamical Properties of Lennard-Jones Molecules. *Phys. Rev.* **1967**, *159*, 98–103. [CrossRef]

35. Davidchack, R.L.; Handel, R.; Tretyakov, M.V. Langevin thermostat for rigid body dynamics. *J. Chem. Phys.* **2009**, *130*, 234101. [CrossRef]

36. Ptak, F.; Almeida, C.M.; Prioli, R. Velocity-dependent friction enhances tribomechanical differences between monolayer and multilayer graphene. *Sci. Rep.* **2019**, *9*, 14555. [CrossRef]